Effects of Corrosion Inhibitor on Corrosion of Al-based Alloys in Ethylene Glycol-Water Coolant Environment

Gwang-Soo Choi, Young-Man Kim[†], and Chan-Jin Park[†]

Department of Materials Science and Engineering, Chonnam National University, 77, Yongbong-ro, Buk-gu, Gwangju 61186, Korea
(Received April 04, 2023; Revised May 15, 2023; Accepted May 16, 2023)

The objective of this study was to investigate the effectiveness of sodium dodecyl benzene sulfonate (SDBS) as a corrosion inhibitor on the pitting corrosion behavior of aluminum alloys used in electric vehicle battery cooling systems within a mixture of ethylene glycol and water (EG-W) coolant. Potentiodynamic polarization testing revealed unstable passive film formation on the aluminum alloys in the absence of SDBS. However, the addition of SDBS resulted in a robust passive film, enhancing the pitting corrosion resistance across all examined alloys. Pitting corrosion was predominantly observed near intermetallic compounds in the presence of Cl? ions, which was attributed to galvanic interactions. Among tested alloys, A1040 demonstrated superior resistance due to its lower areal fraction of precipitates and donor density. The incorporation of SDBS inhibitors mitigated the overall pitting corrosion process by hindering Cl? ion penetration. These findings suggest that SDBS can significantly improve pitting corrosion resistance in aluminum alloys employed in battery coolant environments.

Keywords: *Battery cooling system, Aluminum alloys, Corrosion inhibitor, Intermetallic compounds, Pitting corrosion*

1. Introduction

In an effort to mitigate environmental pollution, there is a push towards electrifying transportation, with a focus on replacing combustion engines and hybrid vehicles with electric vehicles (EVs). One of the challenges to widespread adoption of EVs is the limited lifespan of their batteries, which also poses a risk of fire due to overheating. Automobile manufacturers are actively seeking ways to extend battery life, with a focus on improving thermal management [1-7].

The cooling system for the battery pack is constructed of aluminum alloys, which offer several advantages over other materials [8,9]. These alloys have a lower density compared to carbon steel, which can improve fuel efficiency, and their high thermal conductivity allows for rapid transfer of heat from the battery to the coolant. Aluminum alloys also have high corrosion resistance, as a passive film forms on their surface [10,11].

The coolant used in the battery pack cooling system is a 1:1 mixture of ethylene glycol and water (EG-W).

However, EG is known to be corrosive to aluminum alloys and can prevent the formation of a stable passive film [12-15]. To address this issue, a small amount of sodium dodecyl benzene sulfonate (SDBS), an organic corrosion inhibitor [16,17], was added to the coolant. The impact of the aluminum alloy, SDBS, and the coolant mixture was studied using various techniques, including field emission scanning electron microscopy (FE-SEM), transmission electron microscopy (TEM), energy dispersive X-ray spectroscopy (EDS), potentiodynamic polarization tests, electrochemical impedance spectroscopy (EIS), Mott-Schottky tests, and X-ray photoelectron spectroscopy (XPS).

The results showed that the addition of SDBS to the EG-W (1:1) coolant mixture led to the formation of a stable passive film on all aluminum alloys studied, and increased resistance to pitting corrosion. It is believed that the organic corrosion inhibitor adsorbed onto the passive film and prevented access by pitting corrosion initiators.

2. Experimental Procedure

2.1. Specimen and solution preparation

In this study, three commercial wrought aluminum

[†]Corresponding author: kimy@jnu.ac.kr, parkcj@jnu.ac.kr
Gwang-Soo Choi: Graduate student, Young-Man Kim: Professor,
Chan-Jin Park: Professor

Table 1. Chemical composition (wt%) of wrought Al alloys studied

Alloys	Components							
	Cu	Si	Fe	Mn	Mg	Zn	Ti	Al
A1060	0.05	0.25	0.41	0.03	-	0.02	0.01	Bal.
A3003	0.10	0.11	0.49	1.08	-	-	0.01	Bal.
A6063	0.05	0.51	0.24	0.07	0.68	0.01	0.02	Bal.

alloys with different compositions (A1060, A3003, and A6063) were evaluated for their susceptibility to corrosion in an ethylene glycol (EG-W, 1:1 vol%) environment, with the addition of corrosion inhibitors. The details of the specimens used in the tests are presented in Table 1. The intermetallic compounds were analyzed for their shape and composition after mirror polishing with 1 um diamond suspension.

For electrochemical testing, a copper wire was attached to the back side of the specimens using silver paste and secured in place with epoxy resin. The specimens underwent cold mounting and were then polished to #2000 with SiC paper and ultrasonically cleaned in ethanol and acetone for 5 min. each. A surface area of 1 cm^2 was exposed by masking the specimens with silicone.

The test environment was synthesized by mixing EG-W (1:1) with the addition of the organic corrosion inhibitor, SDBS. To simulate the scenario of unrefined tap water being mistakenly mixed in, 100 ppm of Cl$^-$ ions were added to make a corrosive environment. The experiments were conducted at a temperature of 30°C and atmospheric pressure of 1 atm.

2.2. Analysis of intermetallic compounds

To determine the presence of intermetallic compounds in the aluminum alloys, the specimens were polished from #400 grit with SiC paper to 1 um with a diamond suspension. The surface was then analyzed using scanning electron microscopy (SEM) with energy-dispersive spectroscopy (EDS) to examine the shape and composition of any intermetallic compounds present. The components and selected area electron diffraction (SAED) pattern of these compounds were further analyzed using transmission electron microscopy (TEM) with EDS for a sample of the aluminum alloy obtained using focused ion beam (FIB).

2.3. Electrochemical analysis

To evaluate the corrosion behavior and rate of the aluminum alloys, a potentiodynamic polarization test was conducted using a three-electrode system. The aluminum alloys served as the working electrodes, a platinum plate as the counter electrode, and a saturated calomel electrode (SCE) as the reference electrode. Three electrochemical tests were performed: a potentiodynamic polarization test, an EIS (Electrochemical Impedance Spectroscopy) test, and a Mott-Schottky test. The polarization curves were used to compare the overall polarization behavior, the stability of the passivation film, and the pitting corrosion potential. The polarization test was initiated at a potential 300 mV below the open circuit potential and was concluded upon the observation of pitting corrosion or a sudden increase in current, with a scan rate of 0.5 mV s^{-1}. The EIS test was used to compare the corrosion resistance (R_p), and the Mott-Schottky test was used to compare the donor density of the passivation film. The EIS test was conducted under open circuit conditions, spanning a frequency range from 0.01 Hz to 10 kHz, using a voltage amplitude of 10 mV.

2.4. Analysis of SDBS adsorption on surface

To verify the adsorption of SDBS, a corrosion inhibitor, on the surface of aluminum alloys in an EG-W environment, X-ray photoelectron spectroscopy (XPS) was employed to investigate the surface characteristics. The passive film on the aluminum alloys was formed in an EG-W + SDBS (10 mM) environment and analyzed after 12 h of immersion.

3. Results and Discussion

3.1. Microstructural analysis of aluminum alloys

The shape of intermetallic compounds can be differentiated through the contrast in the back scattered electron (BSE)
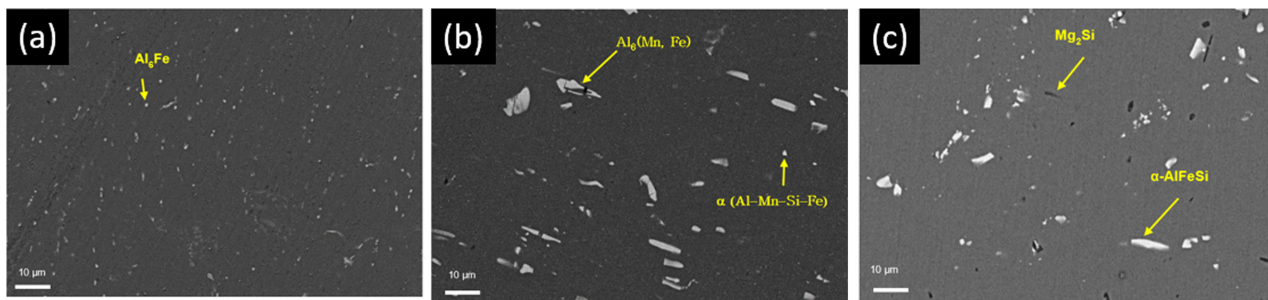
Fig. 1. Back-scattered electron (BSE) images of (a) A1060, (b) A3003, and (c)A6063

image. The BSE image is brighter for compounds with higher weight ratio when scanned by electrons, thus allowing for distinction based on compound composition. Fig. 1a shows the BSE image of alloy A1060, where the phase with high Fe content is identified as Fe_6Al and is distinguished as brighter color. Fig. 1b presents the BSE image of A3003, which detects two different intermetallic compounds. The $Al_6(Mn,Fe)$ phase, a metastable phase, was found due to insufficient heat treatment. Upon sufficient heat treatment, it transforms into the a primary phase. Two intermetallic compounds were detected in A6063 as shown in Fig. 1c. The Mg_2Si phase was expressed in dark gray due to the small weight difference between Al and Mg, while the a primary phase appeared white under the influence of Fe content. The areal fraction of intermetallic compounds was compared as presented in Table 2, with the results indicating a low fraction in the order of A1060, A6063, and A3003. The areal fraction

of intermetallic compounds in A3003 was found to be about four times higher than that of A1060, leading to a higher susceptibility to pitting corrosion in A3003 alloys.

To further characterize aluminum alloy A3003, a specimen prepared by FIB was analyzed using TEM-EDS and selected area electron diffraction (SAED). Fig. 2 presents the mapping images, which primarily consist of aluminum components and include elements such as Fe, Mn, and Si. The $Al_6(Mn, Fe)$ was smaller in size and had an elliptical shape, found at the grain boundaries, whereas the alpha phase was larger, circular, and of a similar size to the aluminum grain. Figs. 3a-c and Figs. 3d-g show the TEM image, EDS spectrum, and SAED pattern,

Table 2. Areal fraction of intermetallic compounds in the Al alloys

Alloys	A1060	A3003	A6063
Areal fraction (%)	1.24	4.1	2.04
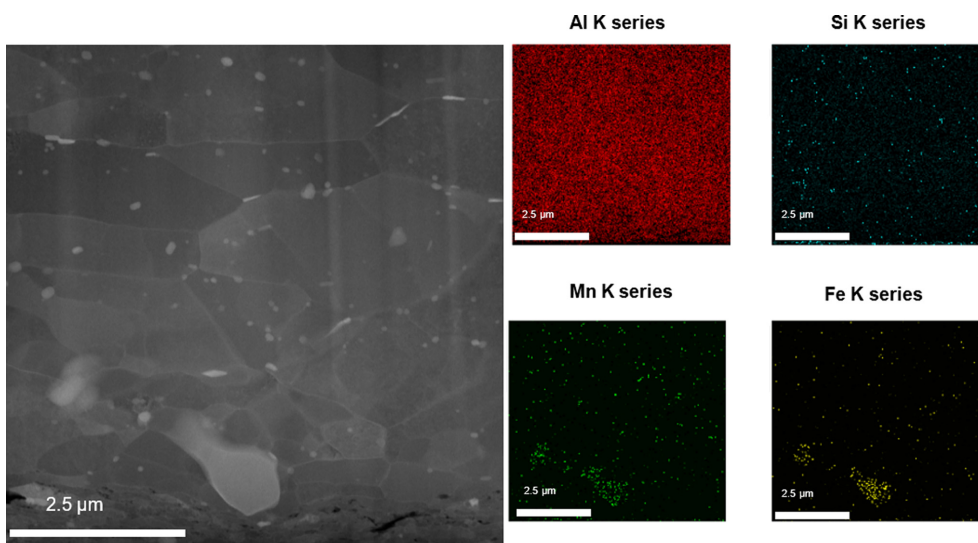
Fig. 2. Scanning TEM image and the corresponding EDS mapping of A3003 alloy
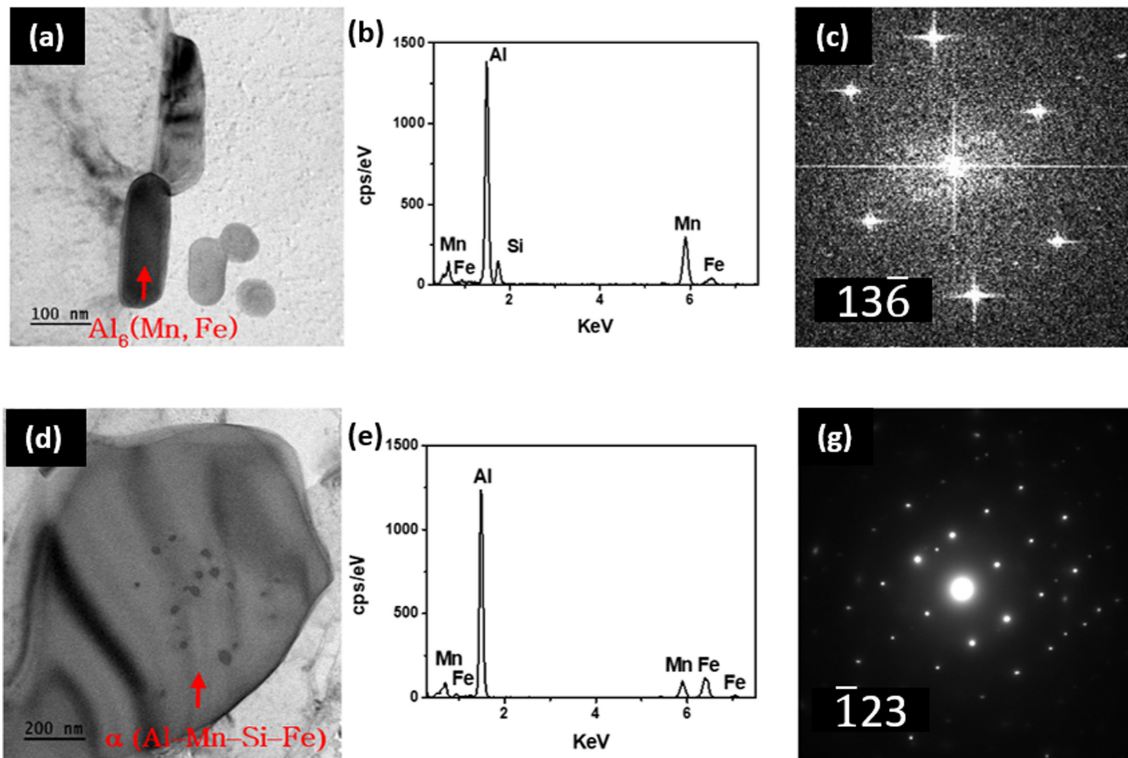
Fig. 3. (a, d) TEM images, (b, e) EDS spectra, (c, g) selected area diffraction patterns of Al_6(Mn, Fe) and a (Al-Mn-Si-Fe) phases

confirming the hexagonal close packing (HCP) structured Al_6(Mn, Fe) and face centered cubic (FCC) structured primary a phases, respectively.

3.2. Anodic polarization of aluminum alloys

Potentiodynamic polarization studies were performed on aluminum alloys to assess their overall corrosion behavior and corrosion rate. To examine the impact of SDBS inhibitor, four solutions were prepared with varying inhibitor and chloride ion concentrations. The polarization curves obtained for each solution are depicted in Fig. 4. In the native coolant environment, the aluminum alloys were found to be poorly passivated when a 1:1 solution of EG-W was used, indicating that the passive film was not stable under this condition (Fig. 4a). The corrosion behavior was primarily characterized by general corrosion rather than pitting corrosion. The observed differences in corrosion potentials among the alloys can be attributed to the influence of their respective alloying elements. Specifically, A3003 exhibited the highest corrosion potential (E_{corr}), followed by A1060 and A6063, in that order.

However, when a 10 mM concentration of SDBS inhibitor was added to the reference solution, all of the alloys demonstrated passivity during the potentiodynamic test as shown in Fig. 4b. Notably, the passive current of A3003 was more stable than that of the other alloys. Pitting corrosion was not observed in any of the samples during this test. However, when the concentration of SDBS inhibitor was increased to 100 ppm, all of the alloys experienced severe loss of passivity, even more so than in the reference solution.

Subsequent addition of 10 mM of SDBS inhibitor to the chloride-containing solution resulted in the recovery of passivity for all of the alloys, as presented in Fig. 4c. However, pitting corrosion occurred at high potential ranges. While the pitting potentials (E_{pit}) of A1060 and A3003 were similar, the E_{pit} of A6063 was much lower than these alloys due to its higher density of intermetallic compounds. These results confirm the effectiveness of SDBS inhibitor in improving the corrosion resistance of the aluminum alloys.

After potentiodynamic polarization test, the surface of the aluminum alloys was observed by using SEM in a
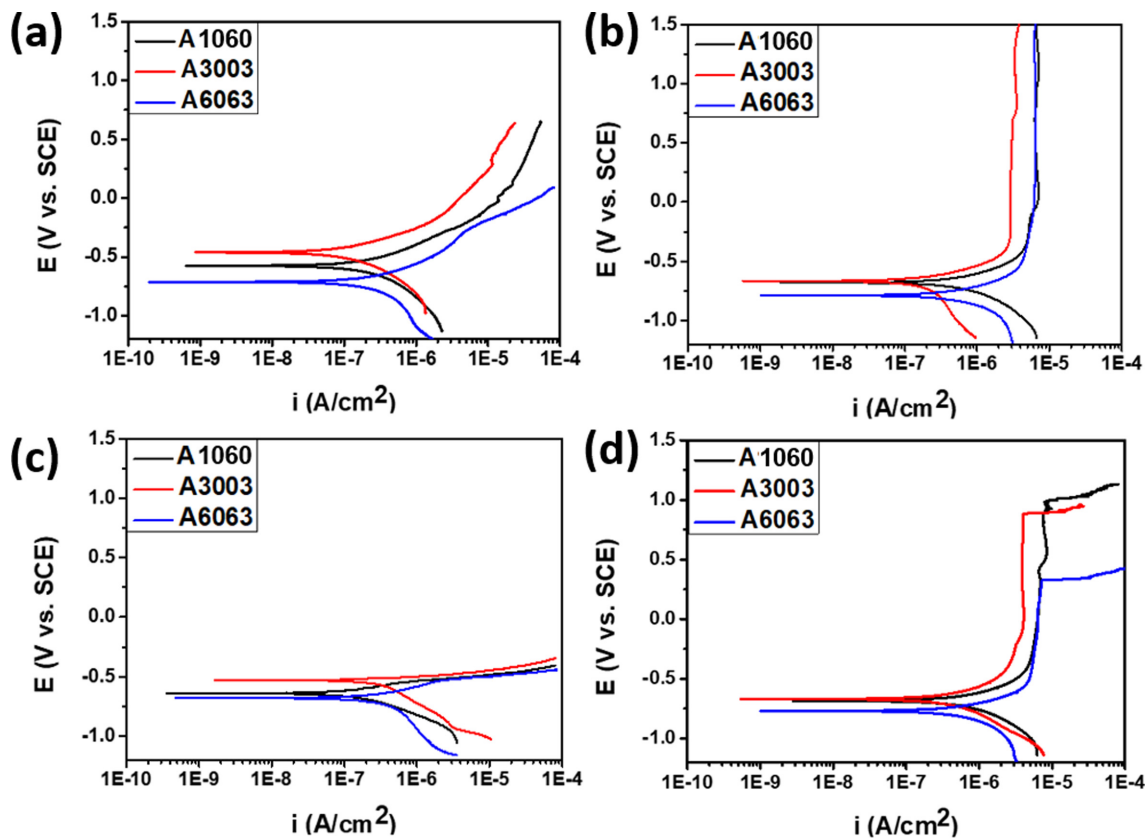
Fig. 4. Anodic polarization curves for A1060, A3003, and A6063 alloys, tested in EG-W (1:1) based solutions: (a) Additive-free, (b) 10 mM SDBS, and (c) 100 ppm NaCl, and (d) 100 ppm NaCl + 10 mM SDBS
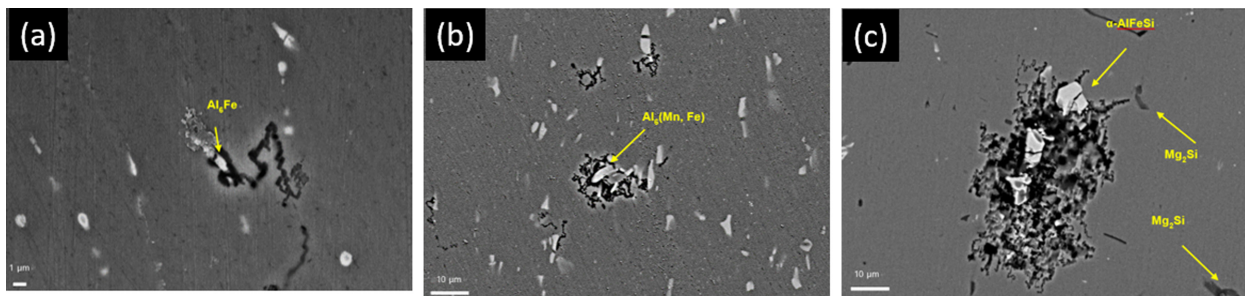
Fig. 5. BSE images showing pitting corrosion around intermetallic compounds in Al alloys. (a) A1060, (b) A3003, and (c) A6063 alloys. The intermetallic compounds are identified by their chemical composition and morphology

BSE mode, as shown in Fig. 5. In A1060 alloy, Al_6Fe phases majorly precipitated as revealed in Fig. 3, and interestingly, pits appeared to occur near the Al_6Fe phases (Fig. 5a). When considering the chemical composition of the Al_6Fe phase and Al matrix, the Al_6Fe phase can be electrochemically nobler than the surrounding matrix. Therefore, pits can initiate around Al_6Fe phases towards Al matrix due to the galvanic action between Al_6Fe phase and Al matrix, in which noble intermetallic compound act as a cathode and surrounding Al matrix can act as
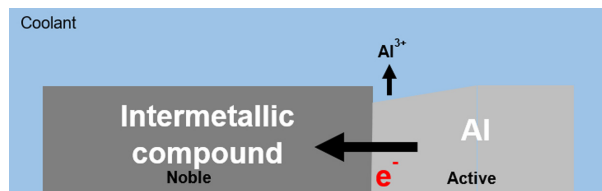
Fig. 6. Schematic illustrating the initiation of corrosion through galvanic action between a nobler intermetallic compound and a more active neighboring Al matrix

anode, as suggested in Fig. 6. Similarly, pits are found around $Al_6(Mn, Fe)$ phases in A3003 alloy (Fig. 5b). The

mechanism for the initiation of pitting corrosion can be also similar in the case of A1004, even though the chemical composition of the intermetallic compound is slightly different between the alloys. For the A3003 alloy, the Al_6Fe phase was found to be more sensitive to pitting corrosion compared to primary a phase. In contrast, for the A6063 alloy, pits were majorly found around primary a phases compared with Mg_2Si phase. It is evident that pits tend to initiate around secondary phases that are large enough to induce depletion or enrichment of alloying elements in the phase boundaries towards the matrix.

3.3. Polarization resistance of aluminum alloys

The electrochemical impedance spectroscopy (EIS) analysis was conducted on various aluminum alloys. Fig. 7ac presents the EIS plots for A1060, A3003, and A6063 alloys, which were measured in ethylene glycol-water (EG-W, 1:1) solutions both with and without the SDBS inhibitor. The equivalent circuit employed for fitting can be found in Fig. 7d. The calculated solution resistance (R_s) and polarization resistance (R_p) values are provided in Table 3. A comparison of the polarization resistance

of the alloys in each environment revealed that, overall, the R_p values of the aluminum alloys measured in the EG-W-based solution containing 10 mM SDBS were considerably larger than those of the aluminum alloys measured in the solution without the inhibitor. As polarization resistance can be considered an indicator of a metal's corrosion resistance, this outcome supports the notion that the corrosion resistance of aluminum alloys can be improved by incorporating the SDBS corrosion inhibitor into the ethylene glycol and water environment. Among the tested aluminum alloys, the R_p values of the

Table 3. Estimated solutions resistance (R_s) and polarization resistance (Rp) values

Alloys	Solutions	R_s (kΩ)	R_p (kΩ)
A1060	EG-W	2.35	131.78
	EG-W + SDBS	0.351	275.63
A3003	EG-W	2.26	174.49
	EG-W + SDBS	0.808	1100
A6063	EG-W	2.49	165.7
	EG-W + SDBS	0.902	455
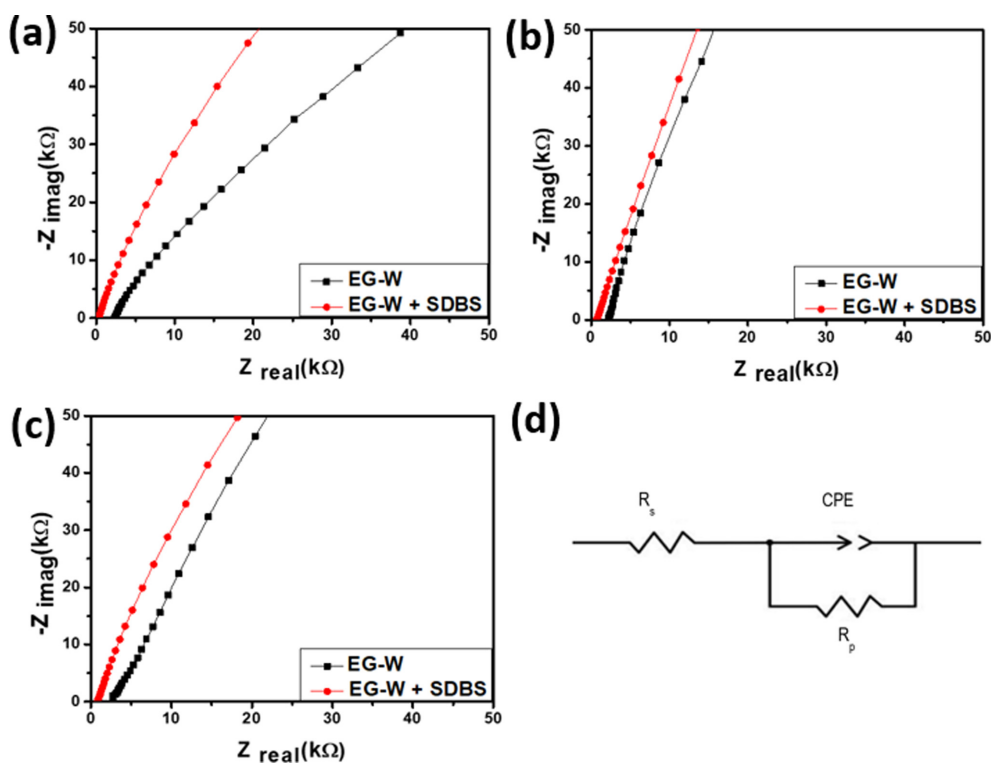
Fig. 7. Electrochemical impedance spectra for (a) A1060, (b) A3003, and (c) 6063, measured in EG-W solutions with and without SDBS inhibitor. (d) indicates the equivalent circuit used for fitting. R_s, and R_p and *CPE* indicate the solution resistance, polarization resistance, and constant phase element, respectively
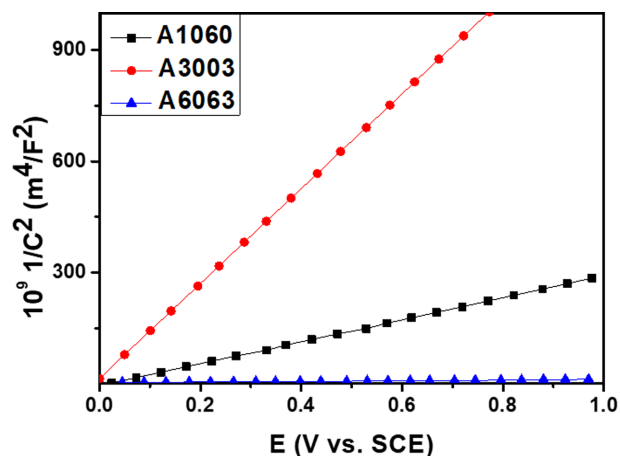
Fig. 8. Mott-Schottky plots for A1060, A3003, and A6063 alloys, measured in EG-W solution containing 10 mM SDBS inhibitor

A3003 alloy were notably larger than those of the other alloys, which is consistent with previous polarization findings.

3.4. Analysis of semiconducting property of passive film on aluminum alloys

After forming a stable passive film on the surfaces of aluminum alloys in an EG-W solution containing 10 mM SDBS, the Mott-Schottky analysis was conducted to investigate the semiconducting properties of the passive films formed on the aluminum alloys, as depicted in Fig. 8. All aluminum alloys exhibited a positive slope, indicating n-type semiconductor properties. Furthermore, the reciprocal of the slope is proportional to the donor density within the passive film. The estimated donor density
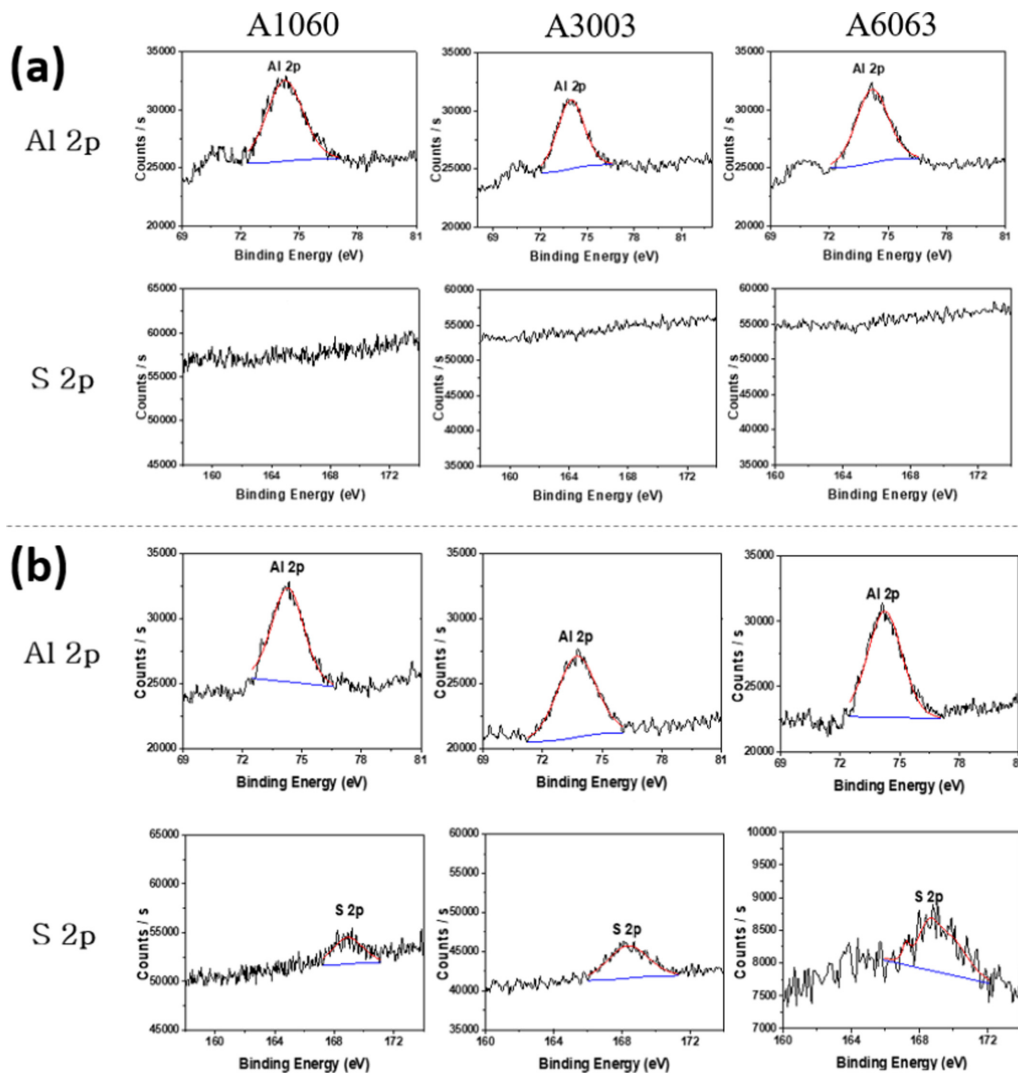
Fig. 9. XPS core spectra corresponding to Al 2p and S 2p for A1060, A3003, and A6063 alloys, observed after 12-hour immersion in EG-W solutions (a) without and (b) with SDBS inhibitor

in the passive film followed the order A6063 > A3003 > A1060. Donor density represents the concentration of oxygen defects in the passivation film, which exhibit cationic characteristics. Consequently, as the donor density in the passivation film increases, the conductivity of the passive film rises, potentially leading to a decrease in corrosion resistance. These findings are consistent with the results obtained for the polarization resistance of the aluminum alloys.

3.5. Analysis of SDBS adsorption on surface

To investigate whether the corrosion inhibitor SDBS was adsorbed on the aluminum alloy surface and a passive film formed in a cooling water environment containing SDBS, XPS analysis was conducted after 12-hour immersion. No sulfur peaks were detected on the surface of aluminum alloys without SDBS (Fig. 9a). In contrast, the presence of a sulfur peak on the surface of aluminum alloys with a stable passivation film formed by adding SDBS (Fig. 9b) confirmed SDBS adsorption. The adsorbed SDBS can hinder the approach of Cl⁻ ions to the aluminum alloy surface, thereby enhancing the corrosion resistance of the aluminum alloys.

4. Conclusions

In this study, we examined the influence of sodium dodecylbenzenesulfonate (SDBS) as a corrosion inhibitor on the pitting corrosion behavior of aluminum alloys employed in battery cooling systems for electric vehicles within a coolant mixture comprising ethylene glycol and water (EG-W) at a 1:1 volume ratio. Potentiodynamic polarization testing demonstrated that the passive film formation on the aluminum alloys was unstable in the coolant mixture. However, with the addition of SDBS, a robust passive film was established on the aluminum alloy surfaces, leading to enhanced pitting corrosion resistance for all examined alloys. Moreover, our analysis revealed that pitting corrosion predominantly occurred in proximity to the intermetallic compounds within the aluminum alloys in an EG-W solution containing Cl⁻ ions, a consequence of the galvanic interaction between the intermetallic compound and the surrounding aluminum matrix. Among the tested alloys, A1060, which exhibited the lowest areal fraction of precipitates and donor density

within the passive film, demonstrated superior pitting corrosion resistance compared to A3003 and A6063. However, the overall pitting corrosion process was mitigated through the incorporation of SDBS inhibitors. The adsorption of SDBS on the aluminum alloy surface effectively obstructed the penetration of Cl? ions, resulting in the suppression of aluminum alloy corrosion. In conclusion, our results indicate that the application of SDBS as a corrosion inhibitor can significantly improve the pitting corrosion resistance of aluminum alloys in battery coolant environments.

References

1. H. Wang, T. Tao, J. Xu, X. Mei, X. Liu, and P. Gou, Cooling capacity of a novel modular liquid-cooled battery thermal management system for cylindrical lithium ion batteries, *Applied Thermal Engineering*, **178**, 115591 (2020). Doi: https://doi.org/10.1016/j.applthermaleng.2020.115591

2. Z. Z. Li, T. H. Cheng, D. J. Xuan, M. Ren, G. Y. Shen, and Y. D. Shen, Optimal Design for Cooling System of Batteries Using DOE and RSM, *International Journal of Precision Engineering and Manufacturing*, **13**, 1641 (2012). Doi: https://doi.org/10.1007/s12541-012-0215-z

3. L. Zhao, J. Wang, Y. Li, Q. Liu, and W. Li, Experimental Investigation of a Lithium Battery Cooling System, *Sustainability*, **11**, 5020 (2019). Doi: https://doi.org/10.3390/su11185020

4. M. Feinauer, N. Uhlmann, C. Ziebert, and T. Blank, Simulation, Set-Up, and Thermal Characterization of a Water-Cooled Li-Ion Battery System, *Batteries-Basel*, **8**, 177 (2022). Doi: https://doi.org/10.3390/batteries8100177

5. K. Chen, Y. Chen, Y. She, M. Song, S. Wang, and L. Chen, Construction of effective symmetrical air-cooled system for battery thermal management, *Applied Thermal Engineering*, **166**, 114679 (2020). Doi: https://doi.org/10.1016/j.applthermaleng.2019.114679

6. X. Wang, S. Liu, Y. Zhang, S. Lv, H. Ni, Y. Deng, and Y. Yuan, A Review of the Power Battery Thermal Management System with Different Cooling, Heating and Coupling System, *Energies*, **15**, 1963 (2022). Doi: https://doi.org/10.3390/en15061963

7. M. Akbarzadeh, T. Kalogiannis, J. Jaguemont, L. Jin, H. Behi, D. Karimi, H. Beheshti, J. V. Mierlo, and M. Berecibar, A comparative study between air cooling and liquid cooling thermal management systems for a high-energy lithium-ion battery module, *Applied Thermal*

Engineering, **198**, 117503 (2021). Doi: https://doi.org/10.1016/j.applthermaleng.2021.117503

8. C. Zhang, Z. Xia, H. Gao, J. Wen, S. Chen, M. Dang, S. Gu, and J. Zhang, A Coolant Circulation Cooling System Combining Aluminum Plates and Copper Rods for Li-Ion Battery Pack, *Energies*, **13**, 4296 (2020). Doi: https://doi.org/10.3390/en13174296

9. Zhonghao Rao, Zhen Qian, Yong Kuang, Yimin Li, Thermal performance of liquid cooling based thermal management system for cylindrical lithium-ion battery module with variable contact surface, *Applied Thermal Engineering*, **123**, 1514 (2017). Doi: https://doi.org/10.1016/j.applthermaleng.2017.06.059

10. D. H. Shin and S. J. Kim, Effects of Chloride Concentration and Applied Current Density on Stray Current Corrosion Characteristics of 6061-T6 Al Alloy for Electric Vehicle Battery Housing, *Corrosion Science and Technology*, **21**, 348 (2022). Doi: https://doi.org/10.14773/cst.2022.21.5.348

11. D. H. Shin and S. J. Kim, Investigation on Electrochemical Characteristics of Battery Housing Material for Electric Vehicles in Solution Simulating an Acid Rain Environment with Chloride Concentrations, *Corrosion Science and Technology*, **21**, 147 (2022). Doi: https://doi.org/10.14773/cst.2022.21.2.147

12. Y. Liu and Y. F. Cheng, Inhibition of Corrosion of 3003 Aluminum Alloy in Ethylene Glycol-Water Solutions, *Journal of Materials Engineering and Performance*, **20**, 271 (2011). Doi: https://doi.org/10.1007/s11665-010-9684-3

13. M. Asadikiya and M. Ghorbani, Effect of Inhibitors on the Corrosion of Automotive Aluminum Alloy in Ethylene Glycol-Water Mixture, *Corrosion*, **67**, 126001 (2011). Doi: https://doi.org/10.5006/1.3666860

14. Y. Liu and Y. F. Cheng, Inhibiting effect of cerium ions on corrosion of 3003 aluminum alloy in ethylene glycol–water solutions, *Journal of Applied Electrochemistry*, **41**, 383 (2011). Doi: https://doi.org/10.1007/s10800-010-0247-y

15. Y. Liu and Y. F. Cheng, Characterization of passivity and pitting corrosion of 3003 aluminum alloy in ethylene glycol–water solutions, *Journal of Applied Electrochemistry*, **41**, 151 (2011). Doi: https://doi.org/10.1007/s10800-010-0215-6

16. J. Y. Sha, H. H. Ge, C. Wan, L. T. Wang, S. Y. Xie, X. J. Meng, and Y. Z. Zhao, Corrosion inhibition behaviour of sodium dodecyl benzene sulphonate for brass in an Al_2O_3 nanofluid and simulated cooling water, *Corrosion Science*, **148**, 123 (2019). Doi: https://doi.org/10.1016/j.corsci.2018.12.006

17. B. H. Shu and J. Xue, Effect of Different Corrosion Inhibitors on Corrosion of AM60B Magnesium Alloy in Simulated Vehicle Coolant, *International Journal of Electrochemical Science*, **17**, 220621 (2022). Doi: https://doi.org/10.20964/2022.06.40